

Suppression of fuel and air stream diluted methane–air partially premixed flames in normal and microgravity

Andrew Lock^a, Suresh K. Aggarwal^{a,*}, Ishwar K. Puri^b, Uday Hegde^c

^aDepartment of Mechanical and Industrial Engineering, University of Illinois at Chicago, Chicago, IL 60607, USA

^bDepartment of Engineering Science and Mechanics, Virginia Polytechnic Institute and State University, Blacksburg, VA 24061, USA

^cNASA Glenn Research Center, Cleveland, OH 44135, USA

Received 1 September 2006; received in revised form 4 December 2006; accepted 27 February 2007

Available online 11 May 2007

Abstract

The effects of fuel and air stream dilution (ASD) with carbon dioxide on the suppression of normal and microgravity laminar methane–air partially premixed coflow jet flames were experimentally and numerically investigated. Experiments were conducted both in our normal-gravity laboratory and at the NASA Glenn Research Center 2.2 s drop tower. Measurements included flame topology and liftoff heights of diluted flames, critical diluent mole fractions for flame blowout, and the radiant heat loss from flames. The flames were also simulated using an axisymmetric unsteady numerical code that utilizes detailed chemistry and transport models. In addition, counterflow flame simulation results were used to examine similitude between the counterflow and coflow flame suppression, and further characterize the effectiveness of fuel stream versus ASD on flame extinction. A smaller relative fuel stream dilution (FSD) extinguishes partially premixed flames (PPFs) with increasing premixing as compared to dilution of the air stream. Conversely, smaller ASD is required to extinguish PPFs as they become less premixed and approach nonpremixed (NP) behavior. Fuel stream diluted PPFs and air stream diluted NP flames extinguish primarily through a reactant dilution effect while fuel stream diluted NP flames and air stream diluted PPF are extinguished primarily by a thermal cooling effect. Normal gravity flames lift off and blow out with a smaller diluent mole fraction than microgravity flames. The difference between the fuel and ASD effectiveness increases as the gravitational acceleration is reduced. Radiation heat losses are observed to increase with increasing diluent mole fraction and decreasing gravity.

© 2007 Elsevier Ltd. All rights reserved.

Keywords: Flame suppression; Partially premixed methane flames; Gravity; Liftoff and blowout

1. Introduction

Halons are excellent fire suppressants. However, concern over the catalytic destruction of ozone by chlorines, bromines and fluorines released into the atmosphere has led to a ban on the production of halon fire suppressants through the Montréal Protocol [1]. Consequently, scientists have been actively exploring halon alternatives that are both environmentally benign and pose a minimum threat to human well being in confined spaces. A variety of chemically active alternatives to halons have been proposed including gaseous fluoromethanes [2] and fluoroethanes [3] as well as various powders [4] and aerosols. Binary agents

which combine the effectiveness of chemically active suppressants mixed with inert gases have also been found quite effective in suppressing flames [5]. However, none of these chemically active agents explicitly fulfills the dual criteria of human safety and being environmentally benign. Consequently, a variety of inert fire suppressants have been investigated, such as water mists [6] and inert gases [7]. Water mists are successfully used in terrestrial applications, but their use in space-based applications is improbable due to water delivery issues as well as the isolation and cleanup of excess water. Therefore, for many applications, the use of an inert gaseous fire suppression agent such as CO₂ is currently the most tractable solution.

It is also important to note that CO₂ is substantially less effective than a chemical agent such as CF₃Br. Bundy and Hamins reported that for air stream dilution (ASD) of

*Corresponding author. Tel.: +1 312 996 2235; fax: +1 312 413 0441.

E-mail address: ska@uic.edu (S.K. Aggarwal).

Nomenclature

ϕ	equivalence ratio
f_{st}	stoichiometric mixture fraction
χ_R	radiant fraction
PPF	partially premixed flame
NPF	nonpremixed flame
FSD	fuel stream dilution

ASD	air stream dilution
$1-g$	normal gravity
$\mu-g$	microgravity
ρ	density
a_s	strain rate
V_1	fuel stream velocity
V_2	air stream velocity

nonpremixed (NP) counterflow flames, CF_3Br is an order of magnitude more effective than CO_2 on volume basis [8], while for fuel stream dilution (FSD), CF_3Br is twice as effective. However, chemically active suppressants, such as CF_3Br , are not used for fire suppression applications due to the health and safety reasons noted earlier.

A large volume of work exists on the effect of fire suppression agents on flames. Extinction of premixed flames has been investigated because the overall reaction rate, heat release and heat and mass transport can be characterized by a single overall parameter, namely, the laminar burning velocity. This has provided a wealth of information which characterizes the decrease in the laminar burning velocity due to (1) radical scavenging in the case of chemically active suppressants [2,3], and (2) through thermodynamic cooling for physically acting, e.g., inert gaseous suppressants [9–11].

Laboratory scale testing of fire suppressants has largely considered the suppressant influence on laminar NP flames since such flames closely mimic the behavior of real fires. NP flame studies have generally involved the suppression of counterflow [8] and cup burner flames [7]. A cup burner or NP jet flame extinguishes through a ‘blow out’ mechanism which decreases the reactivity of the flame base with increasing oxidizer stream dilution [7,12]. In contrast, counterflow flames extinguish through the weakening of the reaction zone that is caused by the dilution of the oxidizer stream. [7,8]. Although these extinction mechanisms appear to be different, counterflow flames have been considered as the limiting case for low stretch jet flames [8,13,14]. Prior to blow out, NP jet flames lift above the burner causing partial premixing of the fuel and air upstream of the flame. This leads to the formation of a partially premixed flame region at the NP flame base. Therefore, it is important to characterize the extinction of partially premixed flames (PPFs) in addition to that of premixed and NP flames.

PPFs are hybrid flames that exhibit the characteristics of both premixed and NP flames [15–17]. Therefore, their extinguishment is not completely described by those for the premixed and NP flame paradigms. A PPF containing multiple reaction zones can be produced by bringing a stream of a fuel rich mixture in contact with air or a fuel lean mixture stream. The spatial variation between the various reaction zones is influenced by the fuel/air equivalence ratio ϕ in the two jets and the overall

hydrodynamics. These reaction zones exhibit the characteristics of either a premixed or a NP flame. For example, a ‘double’ flame with two reaction zones, a RP zone and a NP zone, is produced by placing a fuel rich ($\phi > 1$) jet in contact with an air jet ($\phi = 0$). Similarly, a small premixed region can develop due to upstream mixing at the base of a lifted, diluted, NP flame. Consequently, the propagation and stabilization of this lifted NP flame can then be characterized through a laminar burning velocity, which is also important for the stabilization and extinction of PPFs [18,19].

The most effective location to introduce inert fire suppression agents for NP flames is into their air stream [7,12], while FSD is more effective for premixed flames [20]. The existence of multiple reaction zones in PPFs produces different influences of the FSD and ASD. This is due to the varying importance of the premixed and NP reaction zones that in turn depend upon the local and global values of ϕ . In a previous study we have shown that for a PPF for which $\phi < 2.0$, FSD is more effective at suppressing the flame than ASD. Conversely when $\phi > 2.0$, ASD is more effective [21]. The suppression of PPFs is dependent on the flame structure, which can be changed by varying the partial premixing and the buoyant acceleration [22,23]. Herein, we extend this work to examine how changing the gravitational acceleration affects the relative effectiveness of FSD and ASD in suppressing flames that are established with different levels of partial premixing.

Reducing the gravitational acceleration decreases the advective flow velocity and the flame stretch at the flame base, increases the residence time of the hot gases and, consequently, the radiative heat transfer from the flame [7,11,19,22,24,25]. Katta et al. investigated the effect of gravity on the suppression of methane–air cup burner flames by CO_2 [7]. They showed that a larger CO_2 volume fraction is required in microgravity ($\mu-g$) to destabilize the flame base and subsequently blow out a NP methane–air flame than in normal gravity ($1-g$). Other fundamental studies have considered the microgravity behavior of spherical [11,24,25] and counterflow flames [26]. However, these did not consider the suppression of partially premixed combustion.

The major objective of this experimental and numerical study is to characterize the effect of gravity on the relative effectiveness of FSD versus ASD in suppressing CO_2 -diluted partially premixed and NP methane–air flames

established in coflowing jets. A summary of experimental and numerical findings in the form of critical mole fraction for extinction is presented in Table 1. Experiments were conducted both in our normal-gravity laboratory and at the NASA Glenn Research Center 2.2s drop tower. Flame liftoff heights at different levels of FSD and ASD as well as the critical CO_2 mole fractions required for flame blowout were measured. In addition, the radiation heat transfer from the flames was measured in order to characterize the effect of gravity and CO_2 dilution on flame radiation. The flames were also simulated using an axisymmetric unsteady numerical code that utilizes a detailed chemical kinetics mechanism. In addition, counterflow flame simulation results were used to examine similitude between the counterflow and coflow flame suppression, and to characterize the effects of fuel stream versus ASD on the burning rate and flame suppression.

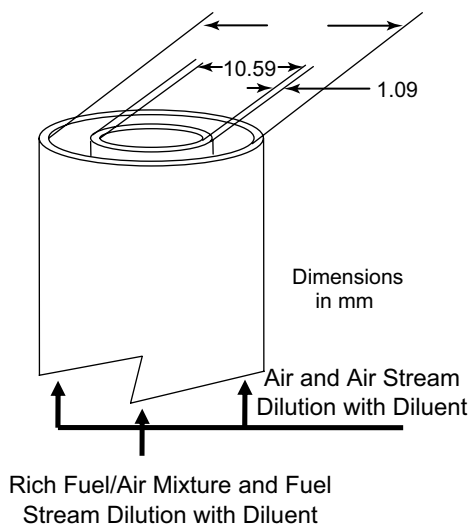
2. Methodology

2.1. Experimental methodology

Experiments were conducted on partially premixed laminar coflowing methane-air jet flames. Two-dimen-

Table 1
Summary of extinction results in terms of the critical CO_2 mole fraction for the extinction of fuel stream diluted (FSD), and air stream diluted (ASD) coflow and counterflow flames

	$\phi = 1.5$		$\phi = 2.25$		$\phi = \infty$	
	FSD	ASD	FSD	ASD	FSD	ASD
1-g coflow X_{CO_2}	0.10	0.30	0.15	0.17	0.11	0.40
μ -g coflow X_{CO_2}	0.12	0.35	0.16	0.20	0.12	0.50
Counterflow $a_s = 100 \text{ s}^{-1}$ X_{CO_2}	0.24	0.42	0.34	0.29	0.71	0.14
Counterflow $a_s = 200 \text{ s}^{-1}$ X_{CO_2}	0.18	0.34	0.24	0.20	0.61	0.09



sional axisymmetric flames were established on a coflow burner that is schematically illustrated in Fig. 1. This flame configuration is somewhat similar to the Burke–Schumann flames [27,28]. The burner consists of two annular tubes. The inner tube has an inner diameter of 11.1 mm with a wall thickness of 1 mm while the outer tube has an inner diameter of 22.2 mm. Several fine mesh screens are inserted into the burner annuli as well as over the face of the burner to develop a plug flow profile at the burner exit. For the cases presented here the inner fuel jet velocity, as well as the coflow air velocities were held at 50 cm/s in order to reduce shear layer effects. The 1-g and μ -g experiments were both performed in our drop rig. It is a flexible self-contained laboratory platform [19,22], an image of which is provided in Fig. 1.

There were two onboard gas bottles that hold the (diluted) fuel and air stream mixtures that were prepared prior to each experiment. The flow was regulated by two MKS mass flow controllers which are accurate to within $\pm 1\%$ of full scale flow. The ignition timing and flow initiation were coordinated by an onboard Tattletale[®] microcontroller and DDAQ system. For microgravity experiments, the gases were premixed in the storage bottles. The rig was loaded into a drop shield and lifted to the top of the drop tower. Once at the top of the tower, all of the rig settings were checked and remote control connections made. The flame was ignited and allowed to stabilize in 1-g as the igniter was retracted. Subsequently, the rig was released and experienced approximately 2.2s of microgravity.

Visual images of the flames were taken using a 640×480 pixel CCD camera mounted in the rig. Video recording was at 30 fps by a MiniDV recorder mounted in the drop tower. A fiber optic cable attached to the rig ran the length of the drop tower to relay the video signal to the recorder. The uncertainty in visual measurements of flame liftoff heights was $\approx 10\%$. Chemiluminescence

Fig. 1. Experimental setup: schematic diagram of coannular burner used for experiments (left), and an image of VT-UIC-NASA Drop Rig (right) used for 1-g and μ -g experiments.

measurements were made for C_2^* at $1-g$ only (due to spatial restrictions in the $\mu-g$ rig) with an Andor iStar intensified CCD camera using a bandpass filter of 470 ± 10 nm wavelength. Radiation measurements were made in $1-g$ with a thermopile type radiometer. This radiometer has a time constant of a second and requires water cooling (so it could also not be effectively utilized in $\mu-g$). The radiometer has a field of view of 150° and was placed 75 mm away from the flame to characterize the global radiation from the entire flame.

2.2. Numerical methodology

The computational model is based on the algorithm developed by Katta et al. [29] and the simulation method is described elsewhere [16,22,30]. It solves the time-dependent governing equations for unsteady reacting flows in an axisymmetric configuration, i.e.,

$$\begin{aligned} \frac{\partial(\rho\Phi)}{\partial t} + \frac{\partial(\rho u\Phi)}{\partial z} + \frac{\partial(\rho v\Phi)}{\partial r} \\ = \frac{\partial}{\partial z} \left(\Gamma^\Phi \frac{\partial\Phi}{\partial z} \right) + \frac{\partial}{\partial r} \left(\Gamma^\Phi \frac{\partial\Phi}{\partial r} \right) - c \frac{\rho v\Phi}{r} + c \frac{\Gamma^\Phi}{r} \frac{\partial\Phi}{\partial r} + S^\Phi. \end{aligned} \quad (1)$$

Here, t denotes the time, and u and v represent the axial (z) and radial (r) velocity components, respectively. The general form of the equation represents conservation of mass, momentum, species, or energy conservation equation, depending on the variable used for Φ . The diffusive transport coefficient Γ^Φ and source terms S^Φ appearing in the equation are provided in Table 1 of Ref. [16]. Introducing the overall species conservation equation and the state equation completes the set of equations. In addition, a sink term based on an optically thin gas assumption is included in the energy equation to account for thermal radiation from the flame [31]. The sink term due to the radiation heat loss is expressed as $q_{\text{rad}} = -4\sigma K_p(T^4 - T_0^4)$ [31], where T denotes the local flame temperature. The term K_p accounts for the absorption and emission from the participating gaseous species (CO_2 , H_2O , CO , and CH_4) and is expressed as $K_p = P \sum_k X_k K_{p,k}$, where $K_{p,k}$ denotes the mean absorption coefficient of the k th species. The methane–air chemistry is modeled using a detailed mechanism that considers 24 species and 81 elementary reactions [32]. This mechanism has been verified with this numerical method for premixed flame speeds and both NP and partially premixed flame structures [16,30,33,34].

A computational domain of $150 \times 100 \text{ mm}^2$ was utilized in the axial (z) and radial (r) directions, respectively. A nonuniform staggered grid of 401×101 grid points was used. This grid was found to be sufficiently refined by sequentially increasing the number of grid points and observing negligible change in the flame shape, structure, and other flame characteristics. The flame was simulated on the same burner shown in Fig. 1 with a nearly flat

burner exit velocity profile which was empirically matched to the experiment. Boundary conditions of symmetry (symmetric axis), outflow (top and outer boundaries), and inflow (base of the domain where gases entered) were used to surround the domain. The top and outer boundaries were situated sufficiently far from the flame to minimize their effect on the simulation. The axisymmetric model has previously been validated against experimental data for a variety of steady and unsteady laminar methane–air flames, including opposed-jet diffusion flames [7], burner-stabilized [15,17,30], lifted [7,35], and both normal and microgravity flames [7,19,22,30,36]. Counterflow flame simulations were conducted using the Chemkin OPDIFF code [37] with the GRI Mech 3.0 chemical kinetics [38]. These simulations were conducted with a separation distance $l = 25.4$ mm. The counterflow flame was centered between the two burner nozzles by balancing the momentum of the opposing flows. The global strain rate $a_s = 2|V_2|/l[1 + (|V_1|\sqrt{\rho_1}/|V_2|\sqrt{\rho_2})]$ was maintained at $a_s = 100 \text{ s}^{-1}$ [28]. The fuel stream and air stream nozzle velocities are V_1 and V_2 , respectively.

3. Results and discussion

Fig. 2 compares the $1-g$ C_2^* chemiluminescence images with the predicted heat release rate contours and velocity vectors for an undiluted and a CO_2 -diluted ($X_{\text{CO}_2} = 0.10$) PPF established at $\phi = 2.25$. The C_2^* chemiluminescence images have been tomographically inverted by use of the Abel inversion [39]. The locations of the various reaction zones and flame liftoff height are predicted reasonably well

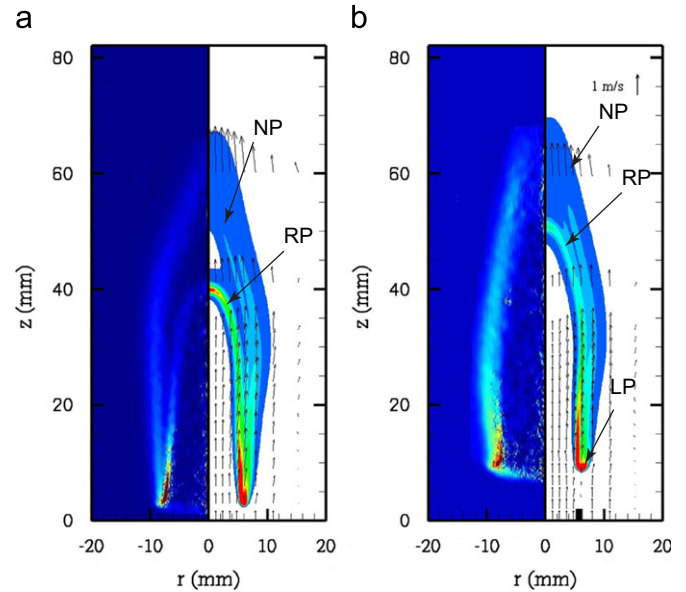


Fig. 2. Comparison of C_2^* chemiluminescence images (left) and predicted heat release rate contours (right) for the undiluted $X_{\text{CO}_2} = 0.0$ and 10% CO_2 -diluted $X_{\text{CO}_2} = 0.10$ PPFs established at $\phi = 2.25$. The RP, nonpremixed, and lean premixed reactions zones are represented by RP, NP, and LP, respectively. The velocity vectors are also shown for the computed flames.

by the numerical model. Both the $1-g$ simulations and measurements exhibited well-organized oscillations that are induced by buoyant acceleration. The oscillation frequency observed in the experiments ranges between 10–15 Hz, while the simulated flames oscillate at frequencies ranging between 8–10 Hz. However, the video images were recorded at 30 Hz, and, therefore, the frequency was poorly resolved in the measurements. In addition, the oscillation frequency was found to be relatively insensitive to ϕ , while the oscillation amplitude was found to increase with increasing ϕ . More detailed discussion about this aspect has been reported in our previous studies [19,23,40]. Because of these buoyancy induced oscillations, care was taken to compare flames at the same phase angle in $1-g$. The $1-g$ undiluted PPF is burner-attached, and, as expected, has a double flame structure [15,23,41,42], containing a rich premixed zone (RP) on the inside and a NP zone outside. Both the measured and predicted flames exhibit this double flame structure, as shown in Fig. 2(a). In contrast the corresponding $1-g$ diluted PPF is lifted above the burner rim and exhibits a triple flame structure at its base, containing a lean premixed (LP) reaction zone in addition to RP and NP. The locations of the three reaction zones, RP, NP, and LP are indicated in Fig. 2(b). Dilution induced lifting of the flame initiates mixing of additional air into the fuel stream [18,40] creating a triple flame structure (containing RP, NP, and LP reaction zones as seen through both the C_2^* image and the simulation. This is a significant feature of such lifted PPFs [15,18,41].

Fig. 3 presents flame images, and simulated heat release rate contours and velocity vectors for $1-g$ PPFs established at $\phi = 2.25$ with both fuel and ASD. The corresponding $\mu-g$ flames are presented in Fig. 4. Tomographically, inverted flames have been presented in Fig. 2 in order to provide a validation of our numerical model. The flame images shown in Figs. 3 and 4, however, are direct visual images which have not been deconvoluted. Nevertheless, there is generally agreement between measurements and simulations for the flames depicted in Figs. 3 and 4. As the PPF is diluted in either the fuel or air stream it slowly lifts off from the burner rim until $X_{CO_2} = 0.10$. Upon further dilution it rapidly moves away from the burner until blow off occurs. There is little difference in the liftoff height between fuel and ASD for the flames shown in Figs. 3 and 4. More significant differences are observed for flames approaching either full premixing ($\phi = 1$) or the NP limit as will be seen later. Despite the similarity in liftoff height, FSD and ASD of the flames induce different changes in the flame structure. With FSD the RP and NP reaction zones merge to a greater degree than with ASD. This can be attributed to the fact that with FSD, the RP zone weakens and shifts towards the NP zone. The $\mu-g$ flames (cf. Fig. 4) are steady because buoyancy induced oscillations are absent. They are established closer to the burner than their $1-g$ counterparts (cf. Fig. 3) due to the effective reduction of the advection flow velocities. Buoyancy induced entrainment is

reduced in $\mu-g$ producing a flame which is both wider and longer [7,22].

3.1. Flame liftoff and blowout

Fig. 5 presents the measured and predicted flame liftoff heights with respect to the CO_2 mole fraction in the fuel and air streams for both $1-g$ and $\mu-g$ flames. Both the measured and the predicted liftoff heights and blowout conditions are presented for flames established at $\phi = 1.5$, 2.25 (PPFs) and ∞ (NPF).¹ Generally good agreement is observed between the experiments and simulations. Both the fuel and air stream diluted flame liftoff heights as well as the critical CO_2 mole fractions at blowout are reasonably well predicted. The quantitative agreement between experimental and numerical liftoff heights deteriorates near blow out. The differences are attributed to the unsteadiness of the $1-g$ near extinction as well as the experimental uncertainties pertaining to the diluent mole fraction. The flame liftoff height is very sensitive to X_{CO_2} near blow out. Additionally, uncertainties in flow boundary condition along with the sensitivity of the simulation to presence of the isothermal insert [15] contribute to the differences.

The undiluted NPF is lifted and stabilized downstream of the burner rim while the undiluted PPFs are stabilized on the burner rim. With FSD, the liftoff height of the NPF first gradually increases followed by more rapid liftoff until blowout occurs. In contrast, both measurements and simulations indicate that the $\phi = 1.5$, and 2.25 PPFs first liftoff from the burner rim due to local dilution-induced extinction [18]. PPFs lifted due to FSD liftoff much more rapidly than the NPF. Consequently, their liftoff heights exceed that of the NPF and the fuel stream diluent mole fractions required for their extinction (through blowout) are significantly smaller than that required for the extinction of the NPF.

The variation of the liftoff height with X_{CO_2} as well as the critical diluent mole fraction at blowout strongly depend on the level of partial premixing, and whether the diluent is added to the fuel stream or air stream. For FSD (ASD), as the level of partial premixing is decreased, i.e., as ϕ is increased, the flame liftoff height decreases (increases) for a given diluent mole fraction, and the critical diluent mole fraction required for extinction increases (decreases). The predicted $1-g$ fuel stream CO_2 dilutions required for blowout of the flames corresponding to Fig. 5 at $\phi = 1.5$, 2.25 and ∞ are $X_{CO_2} = 0.12, 0.16$, and 0.41, respectively. The predicted $1-g$ ASD required for flame blowout at $\phi = 1.5$, 2.25 and ∞ are 0.30, 0.18, and 0.12, respectively. The critical diluent mole fractions for blow out are listed in Table 1. This shows that NPFs are more difficult to extinguish than PPFs with FSD whereas PPFs are more difficult to extinguish with ASD [21].

¹Note that the $\mu-g$ flames at $\phi = 1.5$ and ∞ could not be established in the experimental rig due to safety restrictions on the rig.

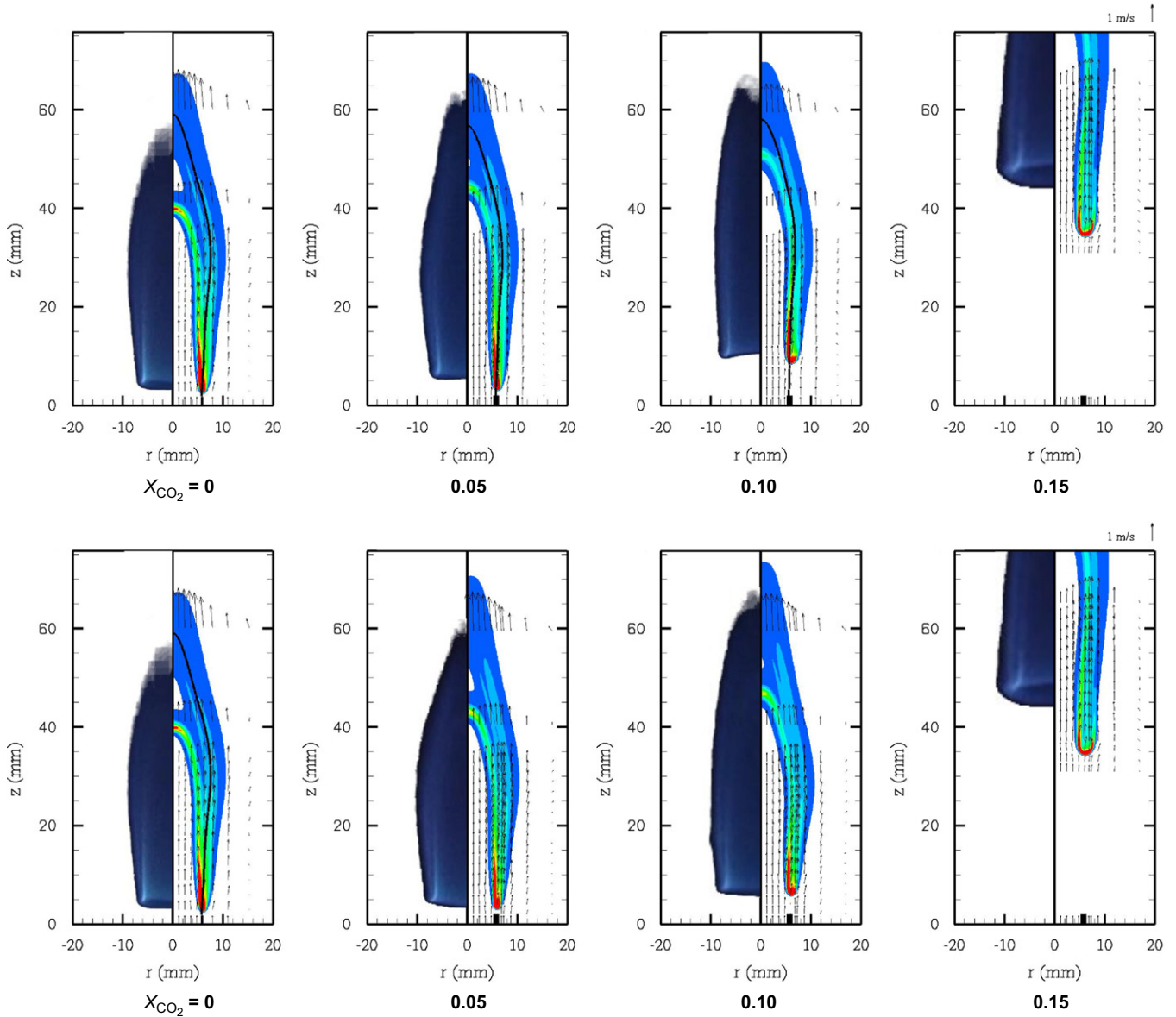


Fig. 3. Comparison of predicted heat release rate contours (right) with measured luminosity contours (left) for normal gravity fuel stream (top) and air stream (bottom) CO₂-diilted $X_{CO_2} = 0.0, 0.05, 0.10, 0.15$ PPFs established at $\phi = 2.25$. Velocity vectors are also shown for the simulated flames.

Another important observation from Table 1 and Figs. 4 and 5 is that both air and FSDs produce similar liftoff heights and critical CO₂ mole fractions for PPFs established at $\phi = 2.25$. This indicates that the $\phi = 2.25$ case is equally susceptible to fuel and ASD and in this respect lies midway between the fully premixed and NP conditions.

Gravitational effects on flame suppression can also be deduced from the results presented Table 2 and Fig. 5. In general, as gravity is reduced, the flame liftoff decreases due to the decrease in buoyant acceleration, and the critical agent mole fraction required for flame blowout (extinction) increases, which is primarily due to the combined effect of reduced buoyant acceleration and increased radiative heat loss from the flame. Perhaps a more important observation in the context of the present study is that the effect of gravity on the flame liftoff height and extinction depends

on the level of partial premixing and whether the suppressant is added to the fuel stream or air stream. For FSD, the effect of gravity becomes more pronounced as the level of partial premixing is reduced, i.e., as ϕ is increased from the premixed limit to the NP limit. In contrast, for ASD, the gravitational effect becomes more pronounced as the level of partial premixing is increased, i.e., as ϕ is reduced from the NP limit to the premixed limit. In addition, the difference between the relative effects of fuel stream and ASDs on flame liftoff and blowout is increased going from $1-g$ to $\mu-g$. For instance, at $\phi = 1.5$, the critical CO₂ mole fraction for FSD is $X_{CO_2} = 0.10$ in $1-g$ and $X_{CO_2} = 0.12$ in $\mu-g$. The critical CO₂ mole fraction for ASD is $X_{CO_2} = 0.30$ in $1-g$ and $X_{CO_2} = 0.35$ in $\mu-g$. The differences between the fuel and ASDs at $1-g$ and $\mu-g$ for the three cases presented in Fig. 5 are listed in Table 2.

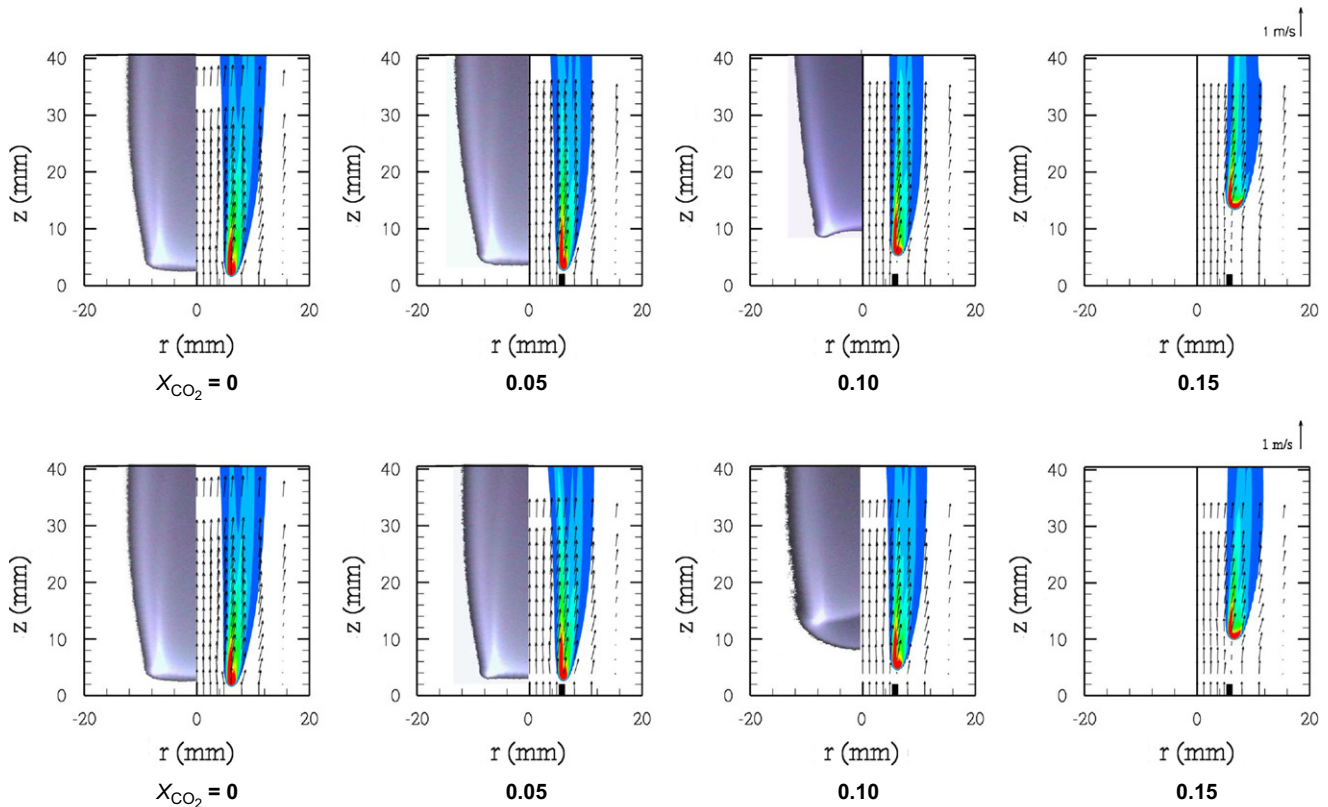


Fig. 4. Comparison of predicted heat release rate contours (right) with measured luminosity contours (left) for microgravity fuel stream (top) and air stream (bottom) CO_2 -diluted $X_{\text{CO}_2} = 0.0, 0.05, 0.10, 0.15$ PPFs established at $\phi = 2.25$. Velocity vectors are also shown for the simulated flames. Flame tips are cropped due to the limited extent of the experimental images.

3.2. Similarity of coflow and counterflow flames

Low strain rate counterflow flames have been shown to extinguish at nearly the same critical diluent mole fraction as low velocity jet flames [7,8,18]. Fig. 6 utilizes this similarity and presents state relationships in terms of major reactant and product species (CH_4 , O_2 , H_2O , and CO_2), and “intermediate” fuel species (H_2 and CO) profiles with respect to the mixture fraction [43,44] for coflow flames established at $\phi = 1.5, 2.25$, and ∞ and counterflow flames established at a global strain rate of 100 s^{-1} and $\phi = 1.5, 2.25$, and 10 . The counterflow flame corresponding to the undiluted NP coflow flame is established at $\phi = 10$ because the coflow flame is slightly lifted above the burner, which causes additional mixing upstream of the flame, producing a nearly merged PPF structure at the flame base [18]. The coflow species profiles are presented for an axial position 2 mm above the flame base. The stoichiometric mixture fraction, f_{st} indicated in the figure represents the flame location.

Despite their different configurations, there is agreement in the scalar profiles for the coflow and counterflow flames. Both types of PPFs established at $\phi = 1.5$ exhibit a double-flame structure (cf. Fig. 6). The PPF established at $\phi = 2.25$ and the NPF also show a similar flame structure in terms of the relative locations of the consumption of reactants and the peak intermediate species. As the partial

premixing decreases (i.e., ϕ increases from 1.5 to ∞), the stoichiometric mixture fraction decreases from $f_{st} = 0.68$ to 0.055 and the RP zone moves from the fuel to the air side. Generally there is better agreement between the coflow and counterflow scalar profiles on the lean side of the flame compared to that on the rich side. The differences on the rich side may be attributable to the different chemistry models used for simulating the coflow and counterflow flames. However, considering that the coflow scalar profiles are plotted only at one axial location, the results exhibit fairly good similarity between the structures of coflow and counterflow flames plotted with respect to the mixture fraction.

A comparison of counterflow flame extinction and coflow flame blow out is presented in Fig. 7. Here, the critical diluent mole fraction for extinction for fuel and air stream diluted counterflow flames is presented versus inverse equivalence ratio, ϕ^{-1} , at two strain rates $a_s = 100$ and 200 s^{-1} . The simulated critical diluent mole fractions for fuel and air stream diluted coflow flame blowout are also presented for both $1-g$ and $\mu-g$. We see that PPFs are more easily extinguished with FSD whereas the NPF responds to ASD. The efficacy of fuel or ASD changes at $f_{st} = 0.5$. This is a transition point because the deficient reactant represents the reactant stream in which dilution becomes the determining factor as to whether fuel or ASD is more effective from the perspective of extinction

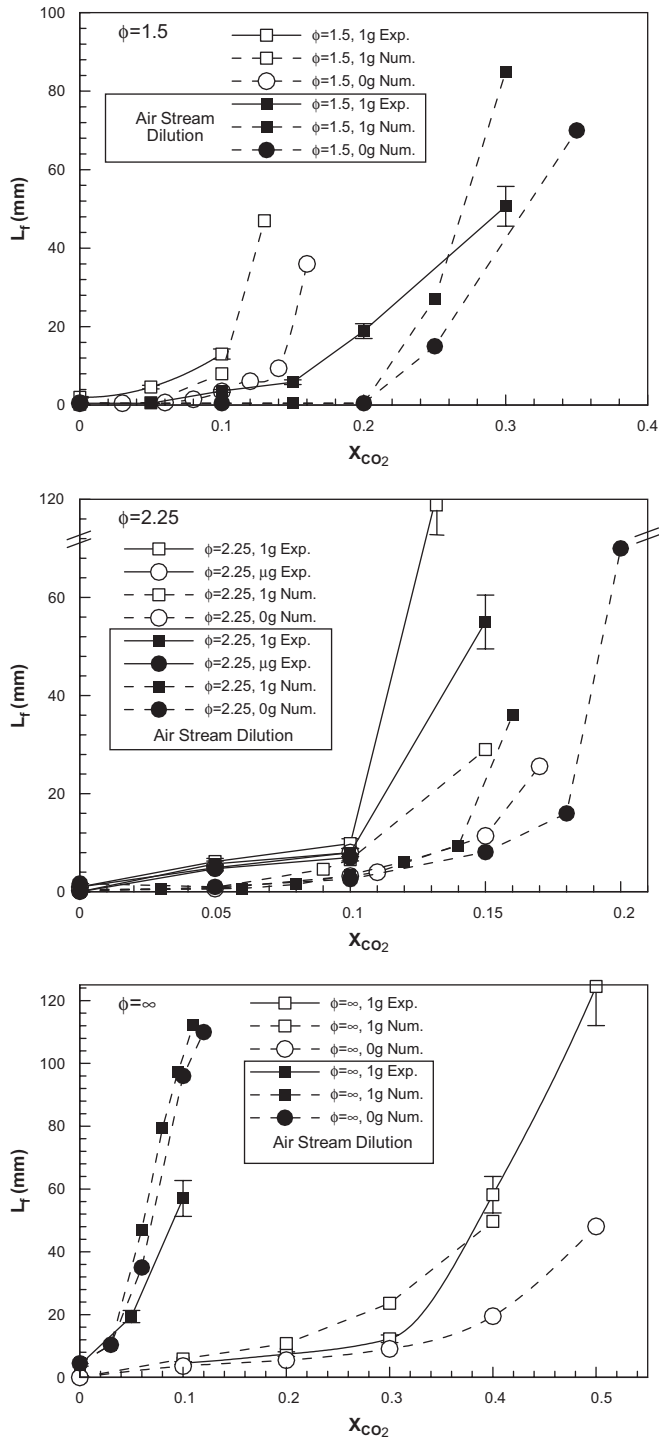


Fig. 5. Measured (solid lines) and predicted (dashed lines) lift-off height (L_f) plotted as a function of CO_2 mole fraction for the fuel (open symbols) and air (closed symbols) stream diluted, normal gravity (squares) and microgravity (circles) coflow PPFs (at $\phi = 1.5$, and 2.25) and NPF. The blowout conditions are also shown.

[21]. Therefore, for $f_{st} < 0.5$, ASD is more effective since air (oxidizer) is the deficient reactant, while for $f_{st} > 0.5$, FSD is more effective since fuel is the deficient reactant.

There are different mechanisms for flame extinction [7,8,45] including: (1) chemical quenching of the flame by

Table 2

Difference between critical CO_2 mole fractions for fuel and air stream dilution at $1-g$ and $\mu-g$

	$1-g$ X_{CO_2}	$\mu-g$ X_{CO_2}
$\phi = 1.5$		
FSD	0.10	0.12
ASD	0.30	0.35
ΔX_{CO_2}	0.20	0.23
$\phi = 2.25$		
FSD	0.15	0.16
ASD	0.17	0.20
ΔX_{CO_2}	0.02	0.04
$\phi = \infty$		
FSD	0.11	0.40
ASD	0.12	0.55
ΔX_{CO_2}	0.01	0.15

radical scavenging as in the case of chemically active suppressants such as halon; (2) thermodynamic cooling of the flame by the diluent heat capacity; and (3) reducing the reactant concentration by introducing a diluent [45]. Because CO_2 is for the most part chemically inert [46], its important suppression effects are through thermal cooling and dilution. Based on observation that the more effective dilution delivery is always in the deficient reactant stream, we conclude for both counterflow and coflow flames, suppression by dilution in addition to thermal cooling is more effective than thermal cooling alone [21].

Fig. 7 includes $1-g$ and $\mu-g$ results for coflow flames. The difference in the critical values of X_{CO_2} between $1-g$ and $\mu-g$ at blowout is a function of the equivalence ratio. For FSD, as ϕ decreases (or ϕ^{-1} increases) the difference between $1-g$ and $\mu-g$ results also decreases, since the flame becomes less dependent upon oxygen transport. As the flame becomes more dependent on oxygen transport when ϕ increases, it is more susceptible to ASD. The difference between the $1-g$ and $\mu-g$ results is largest towards the fully premixed condition for ASD (ϕ decreasing) and minimum towards the NP limit. NP for $1-g$ and $\mu-g$ flames shows little difference in terms of the critical CO_2 mole fraction with ASD. The effect of a change in the gravitational acceleration is small depending on the diluent delivery location. There is only a small difference between $1-g$ and $\mu-g$ PPFs for FSD at near stoichiometric conditions, and when NPFs are subjected to ASD.

3.3. Effects of fuel and ASD on flame structure

The merging of the RP and NP reaction zones with FSD of a PPF depicted in Fig. 3 is indicative of CO_2 -induced suppression. When the fuel stream is diluted the RP zone moves closer to the NP zone. As the value of X_{CO_2} is increased further, PPFs transition from a double to a merged flame structure near extinction. Conversely, as the

air stream of the PPF is diluted, the RP and NP zones maintain their separation until nearly blow out conditions.

The reason lies in the different extinguishment mechanisms for premixed [11] and NP [7,8,12] flames. FSD can be

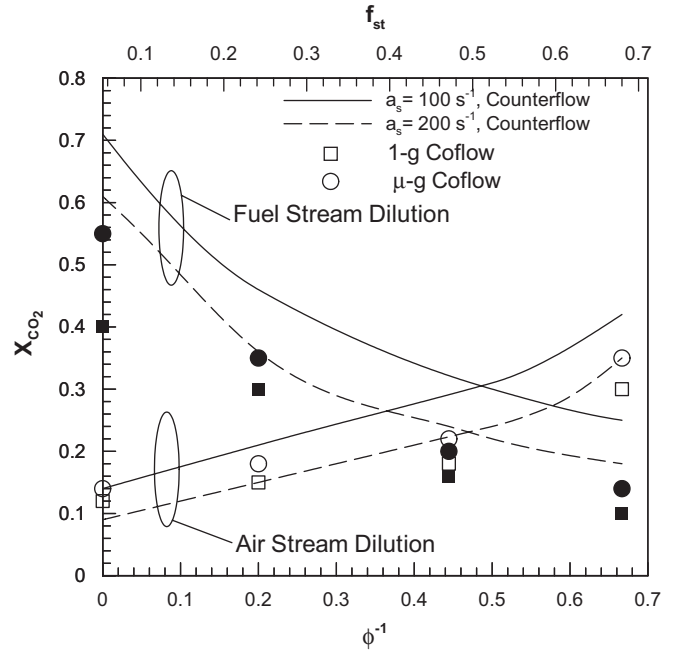
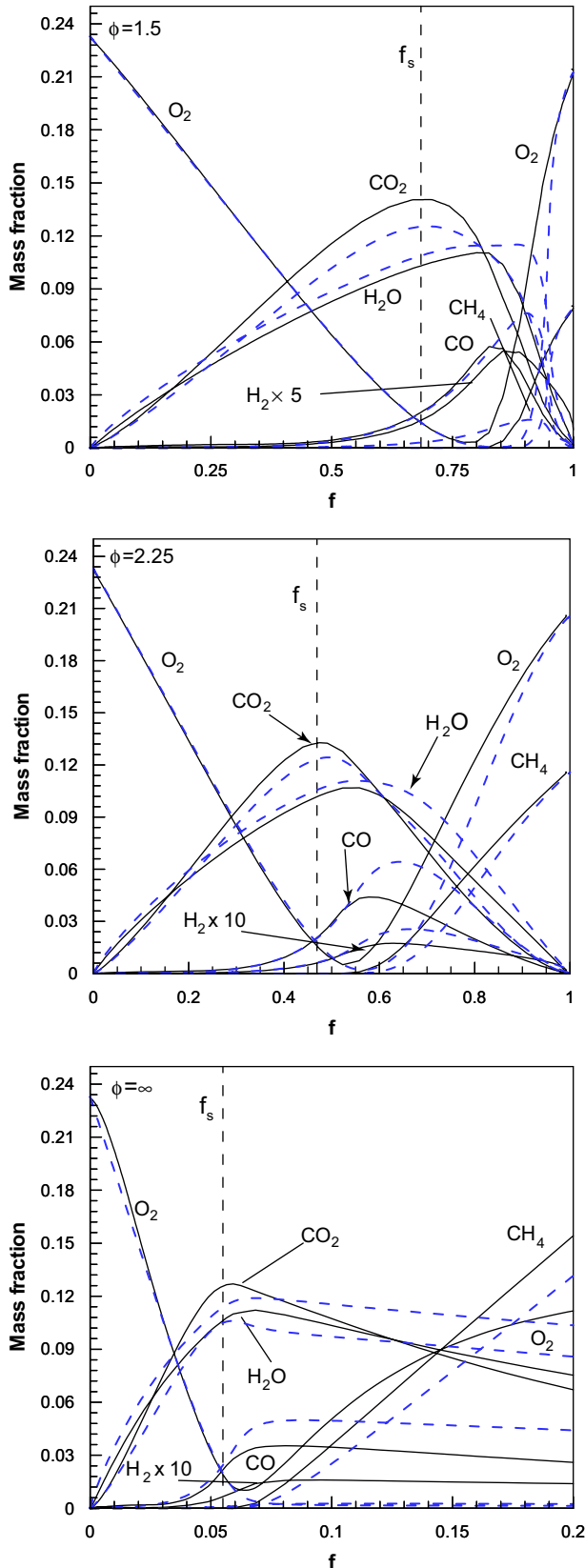


Fig. 7. Critical CO_2 mole fraction, required for the extinction of fuel and air stream diluted coflow and counterflow flames, plotted as a function of inverse equivalence ratio, ϕ^{-1} , and stoichiometric mixture fraction, f_s . The squares represent results of the normal gravity coflow flames and the circles represent the corresponding microgravity flames. Closed and open symbols represent, respectively, results for the fuel stream and air stream diluted coflow flames.

expected to have a larger influence on the RP reaction zone due to thermally cooling, dilution of the deficient reactant (fuel), and reduction of the laminar flame speed S_L . This causes the RP zone to move downstream and closer to the NP zone. A similar merging of the reaction zones is observed for counterflow flames. Fig. 8 illustrates the reduction in S_L with X_{CO_2} for fuel and ASD in the context of two counterflow PPFs established at $\phi = 1.5$ and 2.25.

It was shown earlier that for ϕ smaller than ≈ 2.0 or when f_{st} is larger than ≈ 0.5 , FSD of a PPF is more effective than ASD. Therefore it is to be expected that FSD of a $\phi = 1.5$ flame will have a greater relative influence on S_L than for a $\phi = 2.25$ flame, as seen in Fig. 8. The flame speed also decreases with ASD but much more slowly due to two reasons. First, the transport of the air stream CO_2 to the RP zone is slow, and second it acts primarily to thermally cool the flame in this context without inducing a significant dilution effect. The flame speeds for a $\phi = 2.25$ PPF decrease linearly with both fuel and ASD. This again illustrates the near equal effect of fuel and ASD on this

Fig. 6. State relationships in terms of scalar profiles at the relative axial location of $z = (L_{LE} + 2)$ mm, where L_{LE} indicates the liftoff height, with respect to mixture fraction (f) for the coflow PPFs (at $\phi = 1.5$, and 2.25) and NPF ($\phi = \infty$). Analogous steady counterflow partially premixed flames at $\phi = 1.5$, 2.25, and 10 with a global strain rate of $100 s^{-1}$ are also shown for comparison with the coflow PPFs and NPF, respectively. The solid black and dashed blue lines represent results for the coflow and counterflow flames, respectively. The vertical dashed line represents the stoichiometric mixture fraction (f_s).

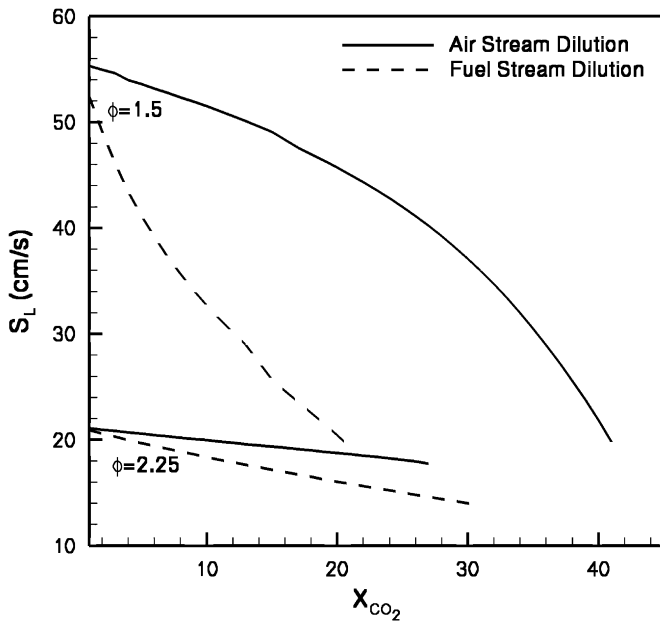


Fig. 8. Stretched flame speed (S_L) plotted as a function of fuel and air stream diluent mole fraction, X_{CO_2} , for counterflow PPFs established at $\phi = 1.5$ and $\phi = 2.25$. Solid and dashed lines represent air and fuel stream dilution of the flame, respectively.

flame. The merger of the RP and NP zones with FSD is caused by the larger effect of FSD on S_L .

3.4. Effect of CO_2 diluent on radiation from the flame

Fig. 9 presents the radiant fraction χ_R , as a function of X_{CO_2} for coflow PPFs established at $\phi = 2.25$ at 1-g and μ -g with fuel and ASDs. The radiant fraction is defined as the ratio the radiant heat transfer rate from the flame to the surroundings \dot{Q}_{rad} to the total heat released by the flame, $\dot{m}_F \Delta h_c$, i.e., $\chi_R = \dot{Q}_{rad} / \dot{m}_F \Delta h_c$ [28]. It indicates the relative importance of radiant heat transfer from a flame. The experimental measurements of χ_R for FSD at 1-g are reasonably well predicted by the simulations as shown in Fig. 9. An offset of $\chi_R \approx 0.05$ in the figure is attributed to discrepancies between the measurement techniques and the numerical calculations. As CO_2 is introduced into either the fuel or the air stream of a flame at 1-g the radiant fraction increases. For a μ -g flame there is a $\chi_R \approx 0.20$ increase that is independent of the quantity of diluent and where it is introduced. The change in χ_R with g is due to the increased residence time in μ -g resulting from the absence of buoyant acceleration [7,22]. As X_{CO_2} is increased, the increase in χ_R for ASD is larger than that for FSD, and these differences become more pronounced at higher dilutions. The difference in χ_R for fuel and air stream diluted flames is due to the amount of diluent being introduced. Since the coflowing annulus of the burner has a larger area, a larger amount of CO_2 is introduced for ASD compared to that for FSD for the same value of X_{CO_2} .

Because the introduction of CO_2 increases χ_R there are two coupled considerations for fire safety. The increased χ_R

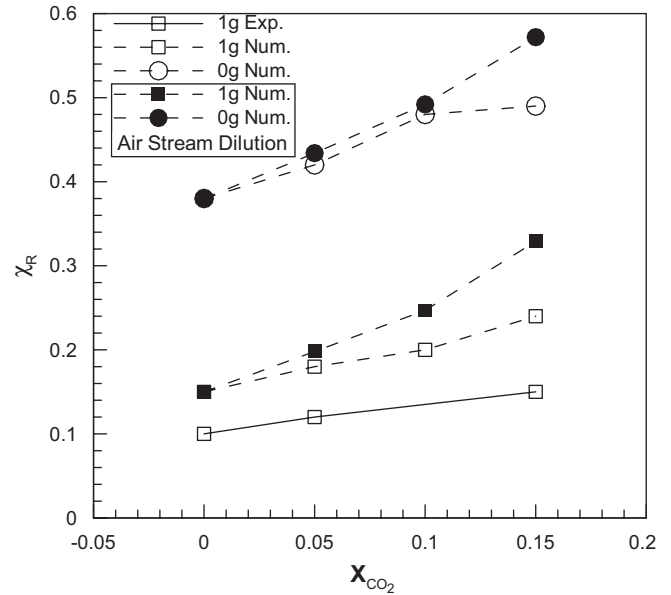


Fig. 9. Radiative heat loss fraction, χ_R , plotted as a function of X_{CO_2} for a PPF established at $\phi = 2.25$ with fuel (open symbols) and air (closed symbols) stream dilution at 1-g (squares) and μ -g (circles). Solid and dashed lines represent experimental measurements and numerical predictions, respectively.

is generally a beneficial effect since it further enhances cooling of the flame in addition to that caused by the thermal capacity of the diluent. However, dilution of the deficient reactant is a more dominant mean of flame suppression than the thermal capacity of the diluent. Since ASD leads to greater radiant heat loss, while FSD is more effective in suppressing PPFs, the increased radiation is unlikely to contribute significantly to the extinguishment of PPFs. On the other hand, the flame is more likely to spread to the surroundings due to enhanced radiation. Consequently, it is especially important to take into account the radiation effect when analyzing fire suppression in μ -g, which may contain regions of partial premixing.

4. Conclusions

We have presented an experimental and numerical investigation of the gravitational effects on the suppression of fuel and air stream diluted partially premixed methane-air flames using CO_2 as the agent. Experiments were conducted both in our normal-gravity laboratory and at the NASA Glenn Research Center 2.2 s drop tower. Measurements included flame topology and liftoff heights of diluted flames, critical diluent mole fractions for flame blowout, and the radiant heat loss from flames. The flames were also simulated using an axisymmetric unsteady numerical code that utilizes detailed chemistry and transport models. In addition, counterflow flame simulation results were used to examine similitude between the counterflow and coflow flame suppression, and further characterize the effectiveness of fuel stream versus ASD on flame extinction.

There is generally good agreement between the measured and predicted flame topologies and liftoff heights for various levels of partial premixing and air stream and FSDs under both $1-g$ and $\mu-g$ conditions. The critical CO_2 mole fractions required for the extinction (blowout) of both $1-g$ and $\mu-g$ flames are also fairly well predicted.

The undiluted NPF is lifted and stabilized downstream of the burner rim while the corresponding PPFs are stabilized on the burner rim. With FSD, the liftoff height of the NPF first gradually increases followed by more rapid liftoff until blowout occurs. The corresponding PPFs liftoff much more rapidly, i.e., their liftoff heights exceed that of the NPF, and extinguish (through blowout) at smaller CO_2 mole fractions than that required for the extinction of NPF. In contrast, with ASD, the NPF is lifted higher than PPFs, and extinguish at smaller CO_2 mole fraction than that required for the extinction of PPFs. Thus FSD is more effective in extinguishing PPFs, while ASD is more effective in extinguishing NPFs.

For fuel stream diluted PPFs, the critical agent mole fraction required for extinction increases as the level of partial premixing is decreased (or ϕ is increased), while for air stream diluted PPFs, the critical agent mole fraction decreases as ϕ is increased. A more detailed analysis indicates that there is transition between the efficacy of FSD and ASD in extinguishing flames at different levels of partial premixing. This transition can be characterized in terms of the stoichiometric mixture fraction (f_{st}) value of ≈ 0.5 . Thus, for $f_{st} < 0.5$, oxidizer is the deficient reactant and ASD is more effective in flame extinguishment, while $f_{st} > 0.5$, fuel is the deficient reactant and FSD is more effective in flame extinguishment. Therefore, the more effective agent delivery is in the deficient reactant stream.

As gravity is reduced, the flame liftoff height decreases while the critical agent mole fraction required for flame extinguishment increases. This is due to the combined effect of reduced buoyant acceleration and increased radiation heat loss from the flame. As ϕ is increased, the effect of gravity on the critical agent mole fraction for extinction becomes more pronounced for FSD, and less pronounced for ASD. Therefore, the difference between the effectiveness of FSD and ASD is increased in the absence of buoyancy.

Despite their different configurations, the scalar profiles of coflow and counterflow flames exhibit similarity with respect to mixture fraction. This implies similarity in the extinction behavior of coflow and counterflow flames, which is confirmed by the computational results.

While radiation heat loss from the flame increases as the gravitational acceleration is reduced and the CO_2 mole fraction is increased, it exhibits greater sensitive to the former.

Acknowledgments

This research was supported by the NASA Office of Physical and Biological Sciences, Microgravity Science

Division, Grant, No. NCC3-688. Special thanks are given to Dr. Kurt Sacksteder who acted as the technical advisor for the NASA GSRP grant which supported Andrew Lock, Gant No. NGT3-52391.

References

- [1] UNEP, Montreal protocol on substances that deplete the ozone layer. 2004.
- [2] Linteris GT, Truett L. Inhibition of premixed methane-air flames by fluoromethanes. *Combust Flame* 1996;105(1–2):15–27.
- [3] Linteris GT, Burgess DR, Babushok V, Zachariah M, Tsang W, Westmoreland P. Inhibition of premixed methane-air flames by fluoroethanes and fluoropropanes. *Combust Flame* 1998;113(1–2):164–80.
- [4] Linteris GT, Katta VR, Takahashi F. Experimental and numerical evaluation of metallic compounds for suppressing cup-burner flames. *Combust Flame* 2004;113(1–2):78–96.
- [5] Saso Y, Ogawa Y, Saito N, Wang H. Binary CF_3Br - and CHF_3 -inert flame suppressants: Effect of temperature on the flame inhibition effectiveness of CF_3Br and CHF_3 . *Combust Flame* 1999;118(3):489–99.
- [6] Seiser R, Seshadri K. The influence of water on extinction and ignition of hydrogen and methane flames. *Proc Combust Inst* 2005;30:407–14.
- [7] Katta VR, Takahashi F, Linteris GT. Suppression of cup-burner flames using carbon dioxide in microgravity. *Combust Flame* 2004;137(4):506–22.
- [8] Bundy M, Hamins A, Lee KY. Suppression limits of low strain rate non-premixed methane flames. *Combust Flame* 2003;133(3):299–310.
- [9] Holley AT, Dong Y, Andac MG, Egolfopoulos FN. Extinction of premixed flames of practical liquid fuels: experiments and simulations. *Combust Flame* 2006;144(3):448–60.
- [10] Modak AU, Abbud-Madrid A, Delplanque JP, Kee RJ. The effect of mono-dispersed water mist on the suppression of laminar premixed hydrogen-, methane-, and propane-air flames. *Combust Flame* 2006;144(1–2):103–11.
- [11] Qiao L, Gu Y, Dahm JA, Oran ES, Faeth GM. Near-limit laminar burning velocities of microgravity premixed hydrogen flames with chemically passive fire suppressants. *Proc Combust Inst* 2006;31 p. xxx–xxx (to appear in).
- [12] Katta VR, Takahashi F, Linteris GT. Fire-suppression characteristics of CF_3H in a cup burner. *Combust Flame* 2006;144(4):645–61.
- [13] Hamins A, Trees D, Seshadri K, Chelliah HK. Extinction of nonpremixed flames with halogenated fire suppressants. *Combust Flame* 1994;99(2):221–30.
- [14] Saso Y, Saito N, Liao CH, Ogawa Y. Extinction of counterflow diffusion flames with halon replacements. *Fire Safety J* 1996;26(4):303–26.
- [15] Azzoni R, Ratti S, Aggarwal SK, Puri IK. The structure of triple flames stabilized on a slot burner. *Combust Flame* 1999;119(1–2):23–40.
- [16] Shu Z, Aggarwal SK, Katta VR, Puri IK. A numerical investigation of the flame structure of an unsteady inverse partially premixed flame. *Combust Flame* 1997;111(4):296–311.
- [17] Shu Z, Krass B, Cho C, Aggarwal SK, Katta V, Puri IK. An experimental and numerical investigation of the structure of steady two-dimensional partially premixed methane-air flames. *Proc Combust Inst* 1998;27:625.
- [18] Briones A, Aggarwal SK, Katta VR. A numerical investigation of flame liftoff, stabilization, and blowout. *Phys Fluids* 2006.
- [19] Lock A, Briones A, Qin X, Aggarwal SK, Puri IK, Hegde U. Liftoff characteristics of partially premixed flames in normal and microgravity. *Combust Flame* 2005;143(3):159–73.
- [20] Qiao L, Kim CH, Faeth GM. Suppression effects of diluents on laminar premixed hydrogen/oxygen/nitrogen flames. *Combust Flame* 2005;143(1–2):79–96.

- [21] Lock A, Briones A, Aggarwal SK, Puri IK, Hegde U. Liftoff and extinction characteristics of fuel and air stream diluted methane–air flames. Submitted to: *Combust Flame* 2006.
- [22] Lock A, Ganguly R, Puri IK, Aggarwal SK. Gravity effects on partially premixed flames: an experimental/numerical investigation. *Proc Combust Inst* 2004;30(30):511–8.
- [23] Qin X, Puri IK, Aggarwal SK, Katta VR. Gravity, radiation, and coflow effects on partially premixed flames. *Phys Fluids* 2004;16(8):2963–74.
- [24] Sunderland PB, Axelbaum RL, Urban DL, Chao BH, Liu S. Effects of structure and hydrodynamics on the sooting behavior of spherical microgravity diffusion flames. *Combust Flame* 2003;132(1–2): 25–33.
- [25] Chernovsky MK, Atreya A, Sacksteder K. The effect of inert substitution on transient spherical diffusion flames in microgravity. In: Technical meeting of the central states section of the Combustion Institute. 2006. Cleveland, OH.
- [26] Maruta K, Yoshida M, Guo HS, Ju YG, Niiooka T. Extinction of low-stretched diffusion flame in microgravity. *Combust Flame* 1998;112(1–2):181–7.
- [27] Burke SP, Schumann TEW. Diffusion flames. *Indus Eng Chem* 1928;20(10):998–1004.
- [28] Turns SR. An introduction to combustion: concepts and applications. New York: McGraw-Hill; 1996.
- [29] Katta VR, Goss LP, Roquemore WM. Effect of nonunity lewis number and finite-rate chemistry on the dynamics of a hydrogen–air jet diffusion flame. *Combust Flame* 1994;96(1–2):60–74.
- [30] Azzoni R, Ratti S, Puri IK, Aggarwal SK. Gravity effects on triple flames: flame structure and flow instability. *Phys Fluids* 1999;11(11): 3449–64.
- [31] Siegel R, Howell J. Thermal radiation heat transfer. London: Taylor and Francis; 2002.
- [32] Peters N, Rogg B. Reduced kinetic mechanisms for applications in combustion systems. Lecture notes in physics, vol. m15, 1993. Berlin: Springer.
- [33] Aggarwal SK, Puri IK, Qin X. A numerical and experimental investigation of “inverse” triple flames. *Phys Fluids* 2001;13(1):265–75.
- [34] Xue HS, Aggarwal SK. Effects of reaction mechanisms on structure and extinction of partially premixed flames. *AIAA J* 2001;39(4):637–45.
- [35] Lee BJ, Chung SH. Stabilization of lifted tribrachial flames in a laminar nonpremixed jet. *Combust Flame* 1997;109(1–2):163–72.
- [36] Takahashi F, Schmoll WJ, Katta VR. Attachment mechanism of diffusion flames. *Proc Combust Inst* 1998;27:675.
- [37] Kee RJ, Rupley FM, Miller JA, Coltrin ME, Grcar JF, Meeks E, et al., CHEMKIN release 4.0.2. 2004. Reaction design.
- [38] Smith GP, Golden DM, Frenklach M, Moriarty NW, Goldenberg BEa, Bowman CT, et al., GRI-Mech 3.0, Internet: <http://www.me.berkeley.edu/gri_mech/>.
- [39] Cho YT, Na SJ. Application of Abel inversion in real-time calculations for circularly and elliptically symmetric radiation sources. *Measure Sci Technol* 2005;16(3):878–84.
- [40] Lock AJ, Ganguly R, Puri IK, Aggarwal SK, Hegde U. Gravity effects on partially premixed flames: an experimental–numerical investigation. *Proc Combust Inst* 2005;30:511–8.
- [41] Qin X, Puri IK, Aggarwal SK. Characteristics of lifted triple flames stabilized in the near field of a partially premixed axisymmetric jet. *Proc Combust Inst* 2003;29:1565–72.
- [42] Shu Z, Choi CW, Aggarwal SK, Katta VR, Puri IK. Gravity effects on steady two-dimensional partially premixed methane–air flames. *Combust Flame* 1999;118(1–2) p. 91–104.
- [43] Aggarwal SK, Puri IK. Flame structure interactions and state relationships in an unsteady partially premixed flame. *AIAA J* 1998;36(7):1190–9.
- [44] Bilger RW. *Proc Combust Inst* 1988;22:475.
- [45] Puri IK. Extinction criteria for buoyant nonpremixed flames. *Combust Sci Tech* 1992;84(1–6):305–21.
- [46] Park J, Hwang DJ, Choi JG, Lee KM, Keel SI, Shim SH. Chemical effects of CO₂ addition to oxidizer and fuel streams on flame structure in H₂–O₂ counterflow diffusion flames. *Int J. Eng Res* 2003;27(13):1205–20.